Article

An N NMR Spin Relaxation Dispersion Study of the Folding of a Pair of Engineered Mutants of Apocytochrome *b*

Wing-Yiu Choy, Zheng Zhou, Yawen Bai, and Lewis E. Kay

J. Am. Chem. Soc., **2005**, 127 (14), 5066-5072• DOI: 10.1021/ja042560u • Publication Date (Web): 19 March 2005

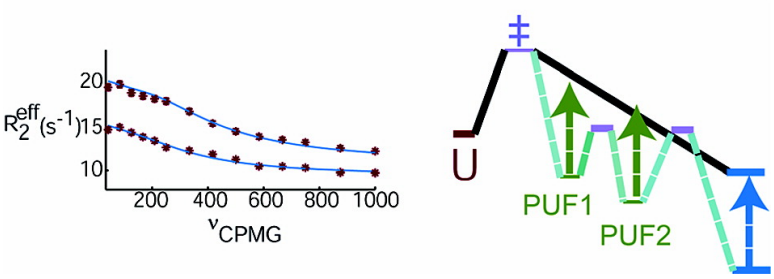

More About This Article

Additional resources and features associated with this article are available within the HTML version:

- Supporting Information
- Links to the 1 articles that cite this article, as of the time of this article download
- Access to high resolution figures
- Links to articles and content related to this article
- Copyright permission to reproduce figures and/or text from this article

View the Full Text HTML

J|A|C|S
ARTICLES
Published on Web 03/19/2005

An ^{15}N NMR Spin Relaxation Dispersion Study of the Folding of a Pair of Engineered Mutants of Apocytochrome b_{562}

Wing-Yiu Choy,[†] Zheng Zhou,[‡] Yawen Bai,[‡] and Lewis E. Kay*,[†]

Contribution from the Protein Engineering Network Centers of Excellence and Departments of Medical Genetics and Microbiology, Biochemistry and Chemistry, University of Toronto, Toronto, Ontario, Canada M5S 1A8, and National Cancer Institute, Laboratory of Biochemistry, Building 37, Room 6114E, Bethesda, Maryland 20892

Received December 10, 2004

Abstract: ^{15}N relaxation dispersion NMR spectroscopy has been used to study exchange dynamics in a pair of mutants of Rd-apocyt b_{562}, a redesigned four-helix-bundle protein. An analysis of the relaxation data over a range of temperatures establishes that exchange in both proteins is best modeled as two-state and that it derives from the folding/unfolding transition. These results are in accord with predictions based on the reaction coordinate for the folding of the protein determined from native-state hydrogen exchange data [Chu, R.; Pei, W.; Takei, J.; Bai, Y. *Biochem*istry **2002**, *41*, 7998−8003]. The kinetics and thermodynamics of the folding transition have been characterized in detail. Although only a narrow range of temperatures could be examined, it is clear that the folding rate temperature profile is distinctly non-Arrhenius for both mutants, with the folding barrier for at least one of them entropic.

Introduction

NMR spectroscopy offers the unique possibility to study protein dynamics at atomic resolution over a broad range of time scales and to relate motion to function.[1−4] Of particular relevance to the work presented here, conformational exchange processes occurring in a protein on the microsecond to millisecond time scale can be probed using a set of relaxation dispersion experiments. These include backbone ^{15}N,[5] ^{1}H,[6] $^{13}C^{\alpha}$,[7] and side-chain methyl ^{13}C[8,9] and ^{15}N (NH_2)[10] single quantum experiments and the recently developed amide double-, zero-[11,12] and ^{1}H−^{15}N or ^{1}H−^{13}C multiple-quantum[9,13] dispersion schemes. These experiments measure the contribution to transverse relaxation rates from the exchange of nuclei between different chemical environments associated with the exchanging conformational states. Parameters such as the rate(s) of exchange and the chemical shift differences between states can be extracted from relaxation dispersion profiles.[14] Most important, the methodology is sensitive to the presence of even a small amount (on the order of 0.5%) of a secondary 'excited' state, so that valuable kinetic and structural information can be obtained on systems under native conditions.[15−19] In many cases such systems cannot be studied using other experimental techniques. One such example involves the folding of G48 mutants of the Fyn SH3 domain that proceeds via low-populated intermediates.[19] In a series of NMR experiments performed at multiple magnetic field strengths and at different temperatures the kinetics and the energetics of the folding processes of a pair of mutational variants of Fyn SH3 have been characterized, along with a qualitative determination of the structures of the intermediates from the extracted chemical shift information.[19]

In this study, we have used ^{15}N relaxation dispersion NMR spectroscopy to study an exchange process occurring in two mutational variants of an engineered apocytochrome b_{562} molecule under native conditions.[20] Cytochrome b_{562} is a four-helix bundle protein with the N- and C− terminal helices tethered by a heme group.[21,22] In the absence of the heme, apocytochrome b_{562} adopts a conformation where the C-terminal

[†] University of Toronto.
[‡] National Cancer Institute.

(1) Palmer, A. G., III. *Chem. Rev.* **2004**, *104*, 3623−3640.
(2) Akke, M. *Curr. Opin. Struct. Biol.* **2002**, *12*, 642−647.
(3) Ishima, R.; Torchia, D. A. *Nat. Struct. Biol.* **2000**, *7*, 740−743.
(4) Kay, L. E. *Nat. Struct. Biol.* **1998**, *5 Suppl*, 513−517.
(5) Loria, J. P.; Rance, M.; Palmer, A. G., III. *J. Am. Chem. Soc.* **1999**, *121*, 2331−2332.
(6) Ishima, R.; Torchia, D. A. *J. Biomol. NMR* **2003**, *25*, 243−248.
(7) Hill, R. B.; Bracken, C.; DeGrado, W. F.; Palmer, A. G., III. *J. Am. Chem. Soc.* **2000**, *122*, 11610−11619.
(8) Skrynnikov, N. R.; Mulder, F. A.; Hon, B.; Dahlquist, F. W.; Kay, L. E. *J. Am. Chem. Soc.* **2001**, *123*, 4556−4566.
(9) Korzhnev, D. M.; Kloiber, K.; Kanelis, V.; Tugarinov, V.; Kay, L. E. *J. Am. Chem. Soc.* **2004**, *126*, 3964−3973.
(10) Mulder, F. A.; Skrynnikov, N. R.; Hon, B.; Dahlquist, F. W.; Kay, L. E. *J. Am. Chem. Soc.* **2001**, *123*, 967−975.
(11) Dittmer, J.; Bodenhausen, G. *J. Am. Chem. Soc.* **2004**, *126*, 1314−1315.
(12) Orekhov, V. Y.; Korzhnev, D. M.; Kay, L. E. *J. Am. Chem. Soc.* **2004**, *126*, 1886−1891.
(13) Korzhnev, D. M.; Kloiber, K.; Kay, L. E. *J. Am. Chem. Soc.* **2004**, *126*, 7320−7329.
(14) Palmer, A. G., III; Kroenke, C. D.; Loria, J. P. *Methods Enzymol.* **2001**, *339*, 204−238.
(15) Mulder, F. A.; Mittermaier, A.; Hon, B.; Dahlquist, F. W.; Kay, L. E. *Nat. Struct. Biol.* **2001**, *8*, 932−935.
(16) Eisenmesser, E. Z.; Bosco, D. A.; Akke, M.; Kern, D. *Science* **2002**, *295*, 1520−1523.
(17) Wolf-Watz, M.; Thai, V.; Henzler-Wildman, K.; Hadjipavlou, G.; Eisenmesser, E. Z.; Kern, D. *Nat. Struct. Mol. Biol.* **2004**, *11*, 945−949.
(18) Grey, M. J.; Wang, C.; Palmer, A. G., III. *J. Am. Chem. Soc.* **2003**, *125*, 14324−14335.
(19) Korzhnev, D. M.; Salvatella, X.; Vendruscolo, M.; Di Nardo, A. A.; Davidson, A. R.; Dobson, C. M.; Kay, L. E. *Nature* **2004**, *430*, 586−590.
(20) Chu, R.; Takei, J.; Knowlton, J. R.; Andrykovitch, M.; Pei, W.; Kajava, A. V.; Steinbach, P. J.; Ji, X.; Bai, Y. *J. Mol. Biol.* **2002**, *323*, 253−262.
(21) Mathews, F. S.; Bethge, P. H.; Czerwinski, E. W. *J. Biol. Chem.* **1979,** *254*, 1699−1706.

10.1021/ja042560u CCC: $30.25

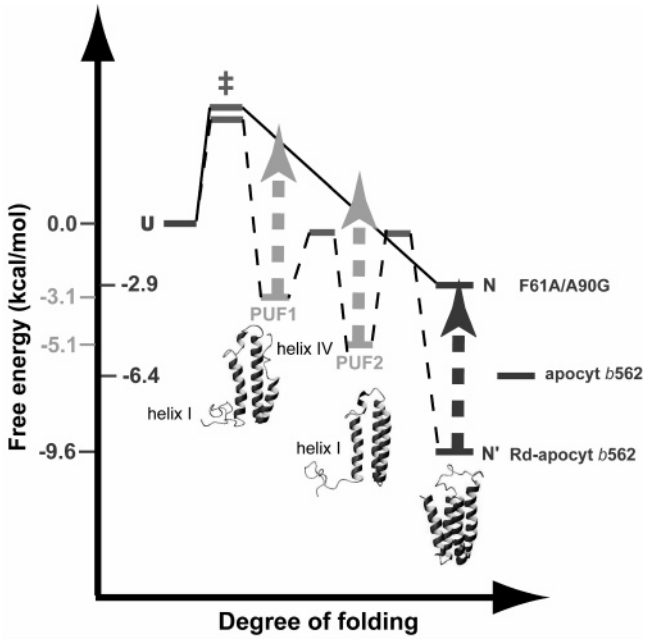

Figure 1. Free energy diagram of the folding pathway for Rd-apocyt b_{562} (redesigned apocytochrome b_{562} with increased stability over the wild-type apo-form, apocyt b_{562}) and its F61A/A90G mutant. The relative energies of U, PUF1, PUF2, N′ (folded, native state of Rd-apocyt b_{562}) have been established by native-state hydrogen exchange experiments[24] and the stability of apocyt b_{562} reported by Fuentes et al.[38] N refers to the folded state of Rd-apocyt b_{562} with the F61A/A90G double mutation. All free energies listed are relative to that of the unfolded state, U. The double mutation (F61A/A90G shown here, or F61A/I72A) destabilizes PUF1, PUF2, and N′ states of Rd-apocyt b_{562} significantly (free energy increases by ~7 kcal/mol), while the U state is unperturbed, as indicated by the vertical arrows in the figure. This causes the free energies of PUF1 and PUF2 to be higher than the unfolded state, and the protein folds in a two-state like manner.

helix unfolds, while the other three helices remain intact.[23] A quintuple mutant (M7W/K98I/N99R/H102N/R106G) of apocytochrome b_{562} has been designed that is more stable than the apo wild type, $\Delta\Delta G_{\text{unfolding}} = 3.2$ kcal/mol, and the folding pathway of this re-designed protein (Rd-apocyt b_{562}) has been extensively characterized using both native-state hydrogen exchange and stopped-flow fluorescence experiments.[20,24] Two partially unfolded conformations (PUFs) that form after the rate-limiting step of folding with stabilities between the unfolded and native states have been found,[24] Figure 1. With knowledge of the reaction coordinate defining the folding process it has become possible to manipulate the structures along the pathway so that they can be studied using standard biophysical approaches. For example, a specific PUF can be populated by destabilizing other states on the folding pathway by mutagenesis so that in effect the PUF becomes the ground state. In this manner the solution structure of one of the PUFs of Rd-apocyt b_{562}, PUF2, has been determined.[20,25] In addition to providing information about intermediates along the pathway, mutations can also be used to test the proposed reaction coordinate itself. For example, the native state hydrogen exchange data provide strong evidence that the N- and C-terminal helices of Rd-apocyt b_{562} are not formed in PUF1, while in PUF2 only the N-terminal helix is not formed.[24,25] Thus, addition of mutations in the other helices that are reportedly structured in the native and in the PUF1/PUF2 states should destabilize all three, Figure 1, without affecting the unfolded ensemble. In the present study two mutational variants of Rd-apocyt b_{562} were designed which destabilize both PUFs and the native state. The prediction is that the free energies of PUF1/PUF2 would now exceed that of the unfolded state so that both PUFs become selectively depopulated and the mutated proteins would therefore fold in a two-state manner. We show here that, in fact, this is the case, providing strong support of the published model of folding of Rd-apocyt b_{562}.[24] In addition, temperature-dependent studies of the folding and unfolding rates of the mutants have allowed the separation of free energy changes into enthalpic and entropic components and provided qualitative estimates for the heat capacity changes that accompany folding.

Materials and Methods

Protein Production. ^{15}N-Labeled mutants, F61A/A90G and F61A/I72A, of Rd-apocyt b_{562} were prepared as described previously.[20,24] Samples were ~1.5 mM in protein, 50 mM NaAc-d_3, pH 4.8.

NMR Spectroscopy. All data sets were recorded on Varian Inova 500 and 800 MHz spectrometers with room-temperature probeheads. The chemical exchange contribution to the transverse relaxation rate of ^{15}N spins was determined from a set of Carr−Purcell−Meiboom−Gill (CPMG) relaxation dispersion spectra[5,26] recorded at 500 and 800 MHz (^{1}H frequency), as described in previous studies.[15,19] Peak intensities, $I(\nu_{\text{CPMG}})$, were obtained from a series of 14 2D ^{15}N−^{1}H correlation maps, measured with values of the CPMG field strength, ν_{CPMG}, ranging from 41.7 to 1000 Hz with constant time relaxation delays, T_{relax}, of either 40 or 48 ms. Two duplicate points for each dispersion series were recorded for error analysis. In addition, reference intensities $I(0)$ were obtained from a spectrum recorded with the constant relaxation time element removed. Each data set comprised 64 × 512 complex points (500 MHz) or 80 × 768 complex points (800 MHz) and [F_1, F_2] spectral widths of [1113 Hz, 8000 Hz] (at 500 MHz) or [1783, 11942 Hz] (at 800 MHz) were employed. Eight scans were recorded per FID with a relaxation delay of 2.0 s. Dispersion profiles were recorded for F61A/A90G at temperatures of 37.5−47.5 °C in 2.5 °C intervals while for F61A/I72A temperature values of 17.5, 20.0, 25.0, 30.0, and 32.5 °C were used.

Data Analysis. Data sets were processed and peak intensities quantified using the NMRPipe software package.[27] Intensities of cross-peaks were converted into effective relaxation rates (R_2^{eff}), via $R_2^{\text{eff}}(\nu_{\text{CPMG}}) = -\ln(I(\nu_{\text{CPMG}})/I(0)) * (1/T_{\text{relax}})$. Uncertainties in R_2^{eff} were calculated based on average standard deviations of peak intensities estimated from repeat measurements (in cases where calculated errors were less than 2% of R_2^{eff}, a minimum value of 2% was used). Dispersion profiles for each well-isolated cross-peak at individual temperatures and magnetic fields were then fit to a two-state exchange model to extract values of R_{ex}, the contribution to the transverse relaxation rate due to chemical exchange. At each temperature, only dispersion profiles with $R_{\text{ex}} > 1.5$ s^{-1} at both magnetic fields were considered for subsequent data analysis. On the basis of this selection criterion, 17(19), 19(17), 32(26), 33(25), and 22(24) cross-peaks at 37.5-(17.5), 40.0(20.0), 42.5(25.0), 45.0(30.0), and 47.5(32.5) °C, respectively, were used in the data analysis for F61A/A90G (F61A/I72A). In-house programs[19] were used for fitting dispersion curves and for the extraction of kinetic and thermodynamic parameters. Values of the model parameters were obtained by least-squares fits of the experimental

(22) Lederer, F.; Glatigny, A.; Bethge, P. H.; Bellamy, H. D.; Matthew, F. S. *J. Mol. Biol.* **1981**, *148*, 427−448.
(23) Feng, Y.; Sligar, S. G.; Wand, A. J. *Nat. Struct. Biol.* **1994**, *1*, 30−35.
(24) Chu, R.; Pei, W.; Takei, J.; Bai, Y. *Biochemistry* **2002**, *41*, 7998−8003.
(25) Feng, H.; Takei, J.; Lipsitz, R.; Tjandra, N.; Bai, Y. *Biochemistry* **2003**, *42*, 12461−12465.
(26) Tollinger, M.; Skrynnikov, N. R.; Mulder, F. A.; Forman-Kay, J. D.; Kay, L. E. *J. Am. Chem. Soc.* **2001**, *123*, 11341−11352.
(27) Delaglio, F.; Grzesiek, S.; Vuister, G. W.; Zhu, G.; Pfeifer, J.; Bax, A. *J. Biomol. NMR* **1995**, *6*, 277−293.

rates ($R^{\text{eff}}_{2,\text{expt}}$) to theoretical values ($R^{\text{eff}}_{2,\text{calc}}$) calculated using analytical expressions,[13] via minimization of a χ^2 target function given by

$$\chi^2 = \sum_i \left[\frac{(R^{\text{eff}}_{2,\text{expt},i} - R^{\text{eff}}_{2,\text{calc},i})}{(\Delta R^{\text{eff}}_{2,\text{expt},i})} \right]^2 \quad (1)$$

where $\Delta R^{\text{eff}}_{2,\text{expt},i}$ is the estimated experimental error. Details of data analysis are as described previously.[19]

Error Analyses. Several different error analyses have been used in this study and are described briefly. In a Monte Carlo analysis[28] experimental data is first fit to the model and a set of theoretical data is then calculated on the basis of the best fit model parameters. Gaussian noise, with the same magnitude as the estimated experimental error, is randomly added to the theoretical data and the resultant data set is subsequently fit to the model. This procedure is repeated n times (in this study, $n = 50$) and the error of each model parameter is calculated as the standard deviation of the parameter values obtained from the n trials. In a bootstrap data analysis,[29] a number of bootstrap samples are randomly generated. Each experimental observation in the original sample is selected (randomly) an arbitrary number of times such that the size of the sample is the *same* as that obtained in the original experiment. 50 bootstrap samples have been used in the analyses described below. Finally, in a jacknife procedure[30] a set of samples are randomly generated and analyzed such that each sample contains only a fraction of the starting data, with the sample size *smaller* than that of the experiment.

Results and Discussion

In this study ^{15}N relaxation dispersion experiments have been used to probe exchange processes in two mutational variants of Rd-apocyt b_{562}, F61A/A90G and F61A/I72A, under non-denaturing conditions (50 mM acetate buffer at pH 4.8). Dispersion profiles for the backbone amide ^{15}N spins have been recorded at two different magnetic field strengths (corresponding to ^{1}H frequencies of 500 and 800 MHz) and over a range of temperatures, as described in Materials and Methods. Most of the profiles measured show significant dispersions, indicating that the amide ^{15}N spins in the protein sense at least one exchange process on the ms time scale. To investigate whether the observed relaxation dispersions are the result of a single dominant exchange process, dispersion profiles of individual residues at each temperature were fit to a two-state model,

$$\mathrm{N} \underset{k_f}{\overset{k_u}{\rightleftharpoons}} \mathrm{U} \quad (2)$$

where N and U correspond to ground and excited states, respectively, and k_f, k_u are the rate constants that describe the exchange process. Errors in rate constants were estimated with a jacknife procedure by which *25% of the data points in each dispersion profile* were randomly removed. The subset of data was subsequently fit to a two-state model to extract values of k_f and k_u on a per-residue basis and the procedure repeated 50 times for each selected residue (based on the selection criteria discussed in the Materials and Methods section). The distributions of values of k_f and k_u for all of the fitted residues are shown in Figure 2 for F61A/A90G and F61A/I72A. In the case

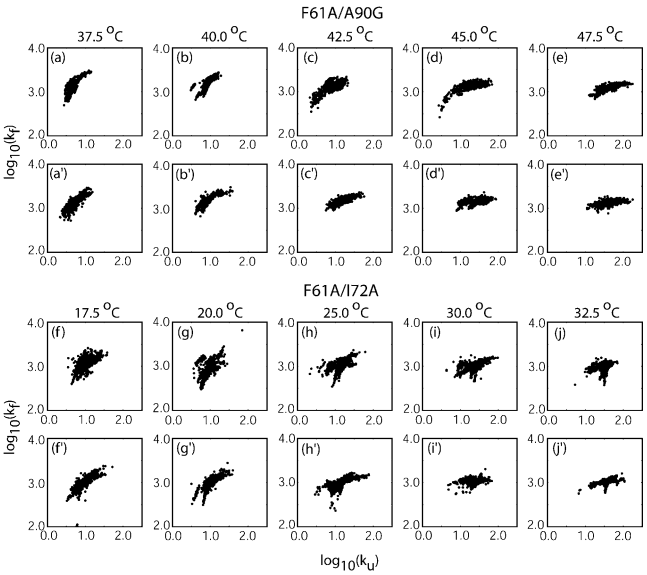

Figure 2. Distributions of k_f and k_u for the F61A/A90G (top) and F61A/I72A (bottom) mutants of Rd-apocyt b_{562}. For each residue used in the data analysis a jacknife procedure[30] was employed to estimate the distributions of experimental data (see text) a−e and f−j. a′−e′ and f′−j′ show the corresponding simulated data, assuming a two-state exchange model and the parameters for chemical shift changes and rates extracted from a global two-state fit of the experimental data.

that the protein dynamics can be described by a single two-state conformational exchange event, all the spin probes should report the same process. By contrast, if the exchange mechanism is more complex (i.e., three-state exchange), fitting of dispersion data to a two-state model is expected to produce residue-specific variations in the parameters describing the exchange process.[19] The relatively narrow distributions of the values of k_f and k_u at each temperature as shown in Figure 2a−e for F61A/A90G and Figure 2f−j for F61A/I72A is consistent with the presence of a single dominant exchange process in each mutant. To estimate the effect of experimental errors on the distributions of k_f and k_u, dispersion data were simulated assuming that *all residues are involved in a single two-state exchange process*. The rate constants for the exchange process and the populations of the excited states at different temperatures, as well as the chemical shift difference between states for each residue in the simulation, were based on the parameters obtained from the global fit of all the experimental dispersion profiles to a two-state model (details discussed below). Gaussian noise based on the estimated experimental errors was added to the simulated data sets, and the same jacknife procedure that was applied to the experimental data was repeated on the simulated data. The distributions of k_f and k_u obtained from the simulations are shown in Figure 2a′−e′ and 2f′−j′ for F61A/A90G and F61A/I72A, respectively. A comparison of the distributions of rate constants from the experimental and simulated data (where a two-state model was explicitly assumed) establishes that the dispersions for both mutants can be explained on the basis of a dominant two-site exchange process, with the widths of the distributions of k_f and k_u determined by the errors in the experimental data.

For each of the two mutants, dispersion profiles of selected residues collected at five different temperatures and two magnetic field strengths were subsequently fit simultaneously to a global two-state exchange model under the following two assumptions: (1) all residues have the same exchange rate

(28) Press: W. H.; Flannery, B. P.; Teukolsky, S. A.; Vetterling, W. T. *Numerical Recipes in C: The Art of Scientific Computing*, 2nd ed.; Cambridge University Press: New York, 1992.
(29) Efron, B.; Tibshirani, R. *Stat. Sci.* **1986**, *1*, 54−77.
(30) Efron, B.; Gong, G. *Am. Stat.* **1983**, *37*, 36−48.

Table 1. Summary of Model Parameters Extracted from Global Fits of the Dispersion Data to a Two-State Exchange Model

temp (°C)	k_{ex} (s^{-1})[a]	k_{ex} (s^{-1})[b]	pU (%)[a]	pU (%)[b]
		F61A/A90G		
37.5	1494 ± 64	1545 ± 73	0.38 ± 0.01	0.37 ± 0.01
40.0	1588 ± 39	1692 ± 53	0.57 ± 0.01	0.56 ± 0.01
42.5	1542 ± 20	1523 ± 25	1.05 ± 0.01	1.03 ± 0.01
45.0	1499 ± 16	1498 ± 18	1.94 ± 0.01	1.91 ± 0.02
47.5	1358 ± 18	1372 ± 19	3.46 ± 0.03	3.60 ± 0.05
		F61A/I72A		
17.5	915 ± 33	1074 ± 39	0.88 ± 0.02	0.80 ± 0.03
20.0	992 ± 38	1037 ± 42	0.94 ± 0.02	0.98 ± 0.03
25.0	1109 ± 25	1131 ± 30	1.44 ± 0.01	1.44 ± 0.02
30.0	1109 ± 15	1106 ± 18	2.61 ± 0.02	2.64 ± 0.03
32.5	1094 ± 11	1085 ± 12	3.53 ± 0.02	3.56 ± 0.04

[a] The exchange rates (k_{ex}) and populations of unfolded states (pU) were obtained from a global fitting of dispersion data at all temperatures and magnetic fields simultaneously. [b] k_{ex} and pU values were obtained from fits of dispersion data at individual temperatures separately.

constants at specific temperatures and (2) for each residue the chemical shift difference between the ground state and the excited state is independent of temperature.[14] The exchange parameters from the global two-state model fit are listed in Table 1. The errors in the exchange rate ($k_{ex} = k_f + k_u$) and the population of the excited state (pU) were estimated using the Monte Carlo analysis described in Materials and Methods. Here theoretical dispersion profiles were generated for each residue based on the fitted exchange parameters and noise added to each curve to generate a new set of profiles that were fit. The process was repeated 50 times with the average and standard deviation in the fitted parameters reported in the table. In general, the dispersion profiles of both mutants fit very well to a global two-state model. Moreover, values of k_{ex} and populations do not depend on whether all of the temperature data is fit together assuming chemical shift differences are temperature invariant, or whether dispersions are fit on a per-temperature basis (compare Table 1, columns *a* and *b*). The one exception is the F61A/I72A mutant at 17.5 °C where significant differences in k_{ex} are noted, likely reflecting the small measured dispersions at this temperature (average $R_{ex} = 3 \pm 0.5\ s^{-1}$ at 500 MHz).

Table 2. Results of the Bootstrap Data Analysis of the Dispersion Data

temp (°C)	k_{ex} (s^{-1})	pU (%)
	F61A/A90G	
37.5	1535 ± 111	0.36 ± 0.02
40.0	1655 ± 70	0.56 ± 0.02
42.5	1517 ± 34	1.03 ± 0.02
45.0	1502 ± 23	1.94 ± 0.03
47.5	1372 ± 29	3.60 ± 0.21
	F61A/I72A	
17.5	1122 ± 122	0.84 ± 0.07
20.0	1045 ± 109	0.99 ± 0.05
25.0	1132 ± 55	1.43 ± 0.04
30.0	1104 ± 29	2.64 ± 0.04
32.5	1080 ± 30	3.59 ± 0.13

Figure 3 illustrates typical fits of dispersion profiles for a representative residue of the F61A/A90G mutant (resonance assignments have not been obtained). The solid line corresponds to the best fit obtained from a global analysis of all residues at all temperatures and magnetic fields using a two-site exchange model. The low reduced χ^2 values (1.1 and 1.6 on average for F61A/A90G and F61A/I72A, respectively) obtained from the two-state model fit suggests that more complex analyses are not warranted. This is consistent with the simulations of Figure 2, where narrow distributions of k_f and k_u are obtained, with the breadth of the distribution due to experimental error. To further elaborate this point, a bootstrap data analysis was performed on the dispersion data.[29] For each mutant, fits of dispersion data at individual temperatures were performed on 50 bootstrap samples generated with randomly selected residues, Table 2. Average values of k_{ex} and pU obtained from the bootstrap analysis are close to those from the two-state model fits *of all data* at individual temperatures, Table 1, consistent

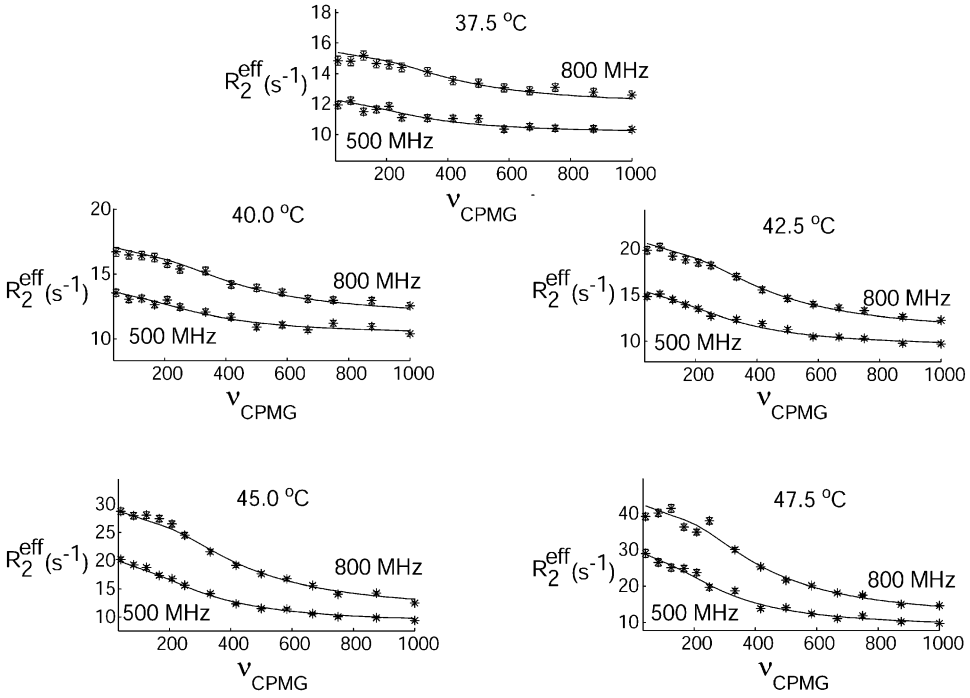

Figure 3. Typical fits of dispersion data from a single residue of the F61A/A90G mutant of Rd-apocyt b_{562} (assignments are not available) using a global two-state model. Dispersion data from all selected residues, all temperatures, and all magnetic field strengths were included in the global fitting.

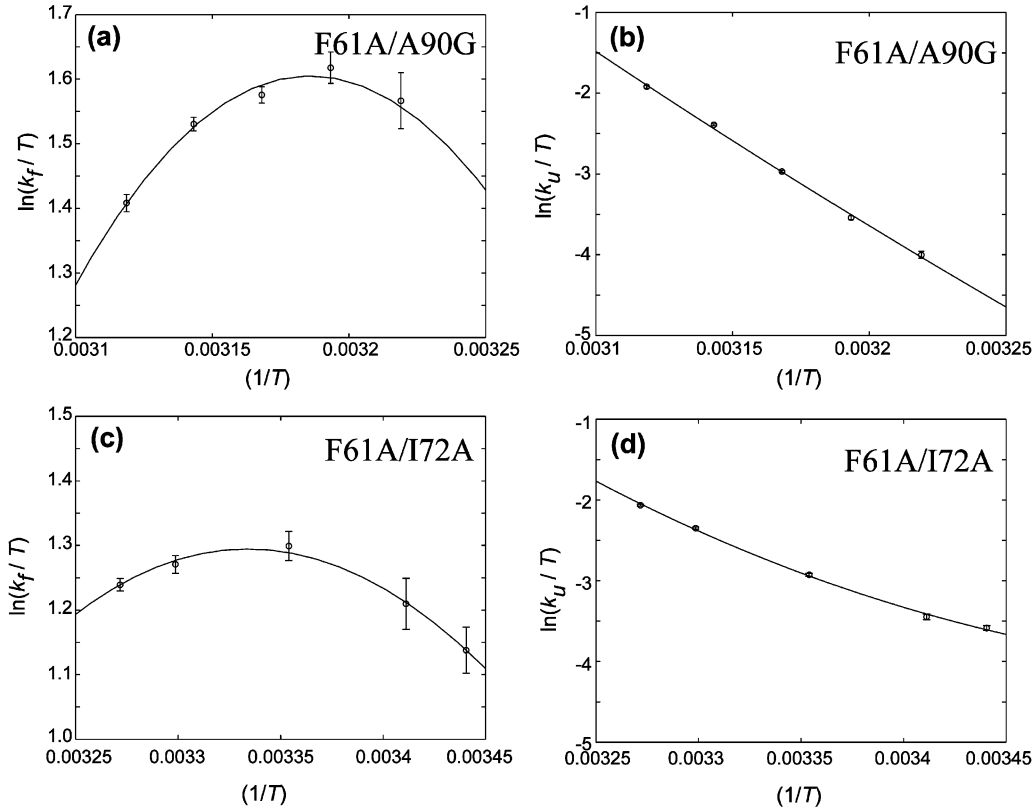

Figure 4. Temperature dependence of the folding and unfolding rates for F61A/A90G (a and b) and F61A/I72A (c and d) shown as Eyring plots. Mean values of ln(k/T) (circles) and errors (vertical lines), obtained via a Monte Carlo analysis are shown, along with the average best fit of the rates in solid lines.

with a single exchange process contributing dominantly to the observed relaxation dispersions for each mutant. Finally, it is of interest to contrast the goodness of the two-state fits of the dispersions recorded for the Rd-apocyt b_{562} mutants considered here (assumed in what follows to be two-state folders) and for the Fyn SH3 domain mutants that we studied previously. In the later case we showed that the exchange process is more complex than two-state.[19] One measure of whether a two-state fit is appropriate is to compare how reduced χ^2 values change between a global (two-state) fit of all of the data ($\chi^2_{r,g}$) vs a fit where each residue is considered on an individual basis and the χ^2 values so obtained summed up (and divided by the total number of degrees of freedom, $\chi^2_{r,g}$). We might expect that the global fit would not be as good as individual fits, in general, since the data has error and there could well be contributions to at least some of the dispersion profiles from additional processes. Nevertheless, in the case of a "two-state" exchange process the ratio of reduced χ^2 values obtained from the two approaches should be close to unity. In the case of the F61A/A90G mutant $\chi^2_{r,g}/\chi^2_{r,i}$ is 1.2, while for F61A/I72A the ratio is 1.1. In contrast, for the Fyn SH3 domain mutants G48M and G48V $\chi^2_{r,g}/\chi^2_{r,i}$ is 2.3 and 3.4, respectively.[19] It is clear that the Fyn SH3 domain folding is more complex than that of Rd-apocyt b_{562}.

The stability differences between excited and ground states can be calculated from their relative populations. On the basis of the values of pU obtained from the global two-state model fits, the excited states of F61A/A90G and F61A/I72A are 2.9 and 2.5 kcal/mol higher in free energy than their corresponding ground states at 42.5 and 25 °C, respectively. These values agree well with the free energy change of folding for the two mutants, determined from thermal-melt experiments using circular dichroism spectroscopy (unpublished data, 2.3 kcal/mol for F61A/A90G at 42.5 °C and 2.4 kcal/mol for F61A/I72A at 25.0 °C). This suggests strongly that the single dominant conformational exchange process detected by the relaxation dispersion experiments for each mutant is indeed the folding/unfolding reaction. Further support is in the form of the significant ^{15}N chemical shift differences ($\Delta\omega_N$) between the ground and excited states obtained from fits of the relaxation dispersion data. For the residues selected for data analysis $\Delta\omega_{N,avg} = 2.8$ ppm (averaged over both F61A/A90G and F61A/I72A mutants) with $\Delta\omega_N$ ranging from ~1.0 to ~7.0 ppm. Finally, the fact that a significant number of residues show exchange (50−60% of the resolved correlations give rise to measurable dispersions) is again consistent with a global folding/unfolding process. In what follows, therefore, the exchange event for both mutants will be viewed in terms of a global protein folding reaction and the parameters k_f, k_u, and pU interpreted accordingly.

The temperature profiles of k_f ($= k_{ex}(1 - pU)$) and k_u ($= k_{ex}pU$) obtained from global fits of the relaxation dispersion curves for the two mutants are shown in Figure 4. It is important to emphasize that the rates are extracted from the data with no assumptions about their temperature dependencies, although they are subsequently fit to the Eyring equation (solid lines, see below). Notably, values of ln(k_u) increase monotonically with temperature for both mutants, while the temperature profiles of ln(k_f) have significant curvature; k_f for each mutant initially increases with temperature and then decreases.

Although many chemical reactions obey Arrhenius theory, $k = A \exp(-E_a/RT)$, where the activation energy E_a is positive, curvature in Arrhenius plots of enzymatic reactions and protein

refolding processes are not uncommon.[31,32] For instance, Oliveberg et al. studied the two-state folding of the protein CI2 over a wide range of temperatures.[31] A strong curvature was observed in the Eyring plot, $\ln(k_f/T)$ vs $1/T$, and the simplest interpretation of this behavior is that there is a large heat capacity change ($\Delta C_p^{\ddagger-U}$) accompanying protein folding.[33] Since a heat capacity change is related to a change in the solvent-accessible surface area of polar and apolar groups in proteins,[34,35] and since the transition state is thought to bury a larger portion of hydrophobic residues than the U state, $\Delta C_p^{\ddagger-U} < 0$. A finite heat capacity change give rises to a temperature dependence of the activation enthalpy of folding as described by

$$\Delta H^{\ddagger-U}(T) = \Delta H^{\ddagger-U}(T_m) + \Delta C_p^{\ddagger-U}(T - T_m) \qquad (3)$$

where T_m is the reference temperature at which $\Delta H^{\ddagger-U}(T_m)$ is determined. According to eq 3, if $\Delta C_p^{\ddagger-U} < 0$, the sign of the activation enthalpy for the folding process can change from positive to negative as the temperature increases, leading to an initial increase in k_f with temperature, followed by a decrease for T values such that $\Delta H^{\ddagger-U}(T) < 0$.

The temperature dependence of k_f,k_u have been fit to the Eyring equation,[36]

$$k_f = (k_B T\kappa/h)\exp(-\Delta G^{\ddagger-U}/RT)$$

$$\Delta G^{\ddagger-U}(T) = \Delta H^{\ddagger-U}(T) - T\Delta S^{\ddagger-U}(T)$$
$$= \Delta H^{\ddagger-U}(T_m) + \Delta C_p^{\ddagger-U}(T - T_m) - T[\Delta S^{\ddagger-U}(T_m) + \Delta C_p^{\ddagger-U}\ln(T/T_m)]$$

and

$$k_u = (k_B T\kappa/h)\exp(-\Delta G^{\ddagger-N}/RT)$$

$$\Delta G^{\ddagger-N}(T) = \Delta H^{\ddagger-N}(T) - T\Delta S^{\ddagger-N}(T)$$
$$= \Delta H^{\ddagger-N}(T_m) + \Delta C_p^{\ddagger-N}(T - T_m) - T[\Delta S^{\ddagger-N}(T_m) + \Delta C_p^{\ddagger-N}\ln(T/T_m)] \quad (4)$$

where k_B and h are Boltzmann and Planck's constants, respectively, κ is the transmission coefficient that is related to the fraction of molecules in the transition state that end up as products, and $\Delta G^{\ddagger-U}(\Delta G^{\ddagger-N})$, $\Delta H^{\ddagger-U}(\Delta H^{\ddagger-N})$, $\Delta S^{\ddagger-U}(\Delta S^{\ddagger-N})$, and $\Delta C_p^{\ddagger-U}(\Delta C_p^{\ddagger-N})$ are the free energy, enthalpy, entropy, and heat capacity differences between the transition state and the unfolded state (folded state), respectively. Figure 5 summarizes the thermodynamic parameters obtained from the fits, with the unfolded state arbitrarily chosen as the reference. It is important to realize that while $\Delta G(= G^N - G^U)$, $\Delta H(= H^N - H^U)$ and $\Delta S(= S^N - S^U)$ are independent of the model used to fit the data (Eyring equation in this case), the values of the activation parameters are not; these values must therefore be interpreted cautiously. This is especially the case since the Eyring formula

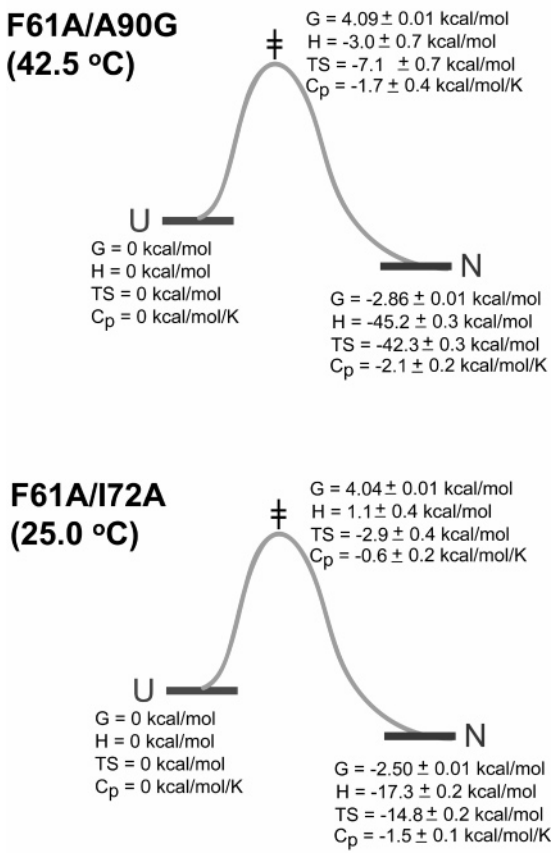

Figure 5. Schematic diagrams of the folding reaction with the thermodynamic parameters of F61A/A90G and F61A/I72A mutants extracted from fits of the temperature dependence of the folding and unfolding rates. The unfolded state of each mutant is used as the reference state. If the data are fit to eq 4 with $\kappa = 1$ (instead of $\kappa = 1.6 \times 10^{-7}$), $G^{\ddagger}$ and $TS^{\ddagger}$ become 13.9 and −16.9 kcal/mol for F61A/A90G and 13.3, −12.2 kcal/mol for F61A/I72A. All other values are unchanged.

was derived for simple chemical reactions, rather than complex, multi-event processes such as those involved in protein folding. Moreover, although ΔG, ΔH, ΔS, and

$$\Delta H^{\ddagger} = -R\frac{\mathrm{d}\ln(k/T)}{\mathrm{d}(1/T)}$$

are independent of κ, $\Delta G^{\ddagger}$ and $\Delta S^{\ddagger}$ do depend on the transmission coefficient. A value of $\kappa = 1.6 \times 10^{-7}$ has been used here, based on an empirical estimate for protein folding,[37] corresponding to $k_B\kappa/h = 3300\ \mathrm{s}^{-1}\ \mathrm{K}^{-1}$.

The thermodynamic parameters for both F61A/A90G and F61A/I72A show the classical and expected entropy−enthalpy compensation,[33] characteristic of protein folding transitions. The activation barrier for folding of F61A/A90G at 42.5 °C is entropic, consistent with studies of other proteins at similar temperatures.[31,32] The significant entropic folding barrier along with a negative $\Delta H^{\ddagger-U}$ may reflect the fact that the transition state is well hydrated and reasonably compact so that many of the enthalpic interactions with water are not lost, while new intramolecular contacts are formed, relative to the unfolded state. At the same time the compaction leads to a reduction in chain entropy that is the major deterrent to folding and hence

(31) Oliveberg, M.; Tan, Y. J.; Fersht, A. R. *Proc. Natl. Acad. Sci. U.S.A.* **1995**, *92*, 8926−8929.
(32) Plaxco, K. W.; Guijarro, J. I.; Morton, C. J.; Pitkeathly, M.; Campbell, I. D.; Dobson, C. M. *Biochemistry* **1998**, *37*, 2529−2537.
(33) Fersht, A. R. *Structure and Mechanism in Protein Science*; W. H. Freeman and Company: New York, 1999.
(34) Murphy, K. P.; Freire, E. *Adv. Protein Chem.* **1992**, *43*, 313−361.
(35) Spolar, R. S.; Livingstone, J. R.; Record, M. T., Jr. *Biochemistry* **1992**, *31*, 3947−3955.
(36) Eyring, H. *Chem. Rev.* **1935**, *17*, 65−77.
(37) Hagen, S. J.; Hofrichter, J.; Szabo, A.; Eaton, W. A. *Proc. Natl. Acad. Sci. U.S.A.* **1996**, *93*, 11615−11617.
(38) Fuentes, E. J.; Wand, A. J. *Biochemistry* **1998**, *37*, 9877−9883.

responsible for the folding barrier. Fersht and co-workers have observed a similar behavior in the k_{ex} vs temperature profile of CI2. In this case k_{ex} decreases for temperatures in excess of ~45 °C, where the folding barrier is the result of the loss in chain entropy upon formation of the transition state.[31] The folding barrier measured for F61A/I72A, 25 °C, is much more balanced with regards to contributions from enthalpy and entropy. The differences between the activation parameters for folding of F61A/A90G and F61A/I72A likely reflect, at least in part, the temperature ranges that were used in the studies (centered about 42.5 vs 25 °C) that were necessary to observe and quantify exchange in the two mutants (see below). The larger (more positive) $\Delta H^{\ddagger-U}$ for F61A/I72A follows directly from eq 3, the significant difference in temperature at which the measurements were made and the negative heat capacity change upon folding ($\Delta C_p^{\ddagger-U}$), while the drop in *TS* from −7 kcal/mol (F61A/A90G, 42.5 °C) to −3 kcal/mol (F61A/I72A, 25 °C) is consistent with the decreased entropic penalty associated with compaction at the lower temperature. Notably, the reversal in folding rate for F61A/I72A occurs at a lower temperature than what has been reported for other proteins,[31,32] Figure 4c.

While it would certainly be of interest to quantify the folding reaction over a larger range of temperatures, the range that is possible is dictated by the size of the dispersion profiles that can be measured. At the lower temperature limit dispersions of only 2−3 s^{-1} are obtained, while at the high-temperature end the increase in the population of the unfolded state leads to large dispersions and a significant decrease in spectral quality. In this regard the narrow temperature window does make it difficult to extract accurate heat capacities and the values reported in Figure 5 are approximate. Indeed in previous temperature-dependent relaxation dispersion studies of conformational exchange in a cavity mutant of T4 lysozyme[15] and in the Fyn SH3 domain[19] the (limited) temperature data was interpreted assuming $\Delta C_p = 0$. It is clear from Figure 4a,c that $\Delta C_p^{\ddagger-U} \neq 0$ for the systems studied here and that $\Delta C_p^{\ddagger-N}$ is also nonzero for F61A/I72A. However, an increase(decrease) in k_f,k_u by 5% for the lowest temperature point only, changes [$\Delta C_p^{\ddagger-U}$,$\Delta C_p^{\ddagger-N}$] significantly, from [−1.7,0.4]kcal/mol/K to [−1.2,0.9] ([−2.1,0.0])kcal/mol/K, for F61A/A90G, for example. Alternatively, an increase(decrease) in k_u alone by 5% changes $\Delta C_p^{\ddagger-N}$ from 0.4 kcal/mol/K to 0.9(0.0) kcal/mol/K (for F61A/A90G), again emphasizing the problems with the limited temperature range that can be explored using this technique.

In conclusion, we have used ^{15}N relaxation dispersion spectroscopy to characterize the folding/unfolding transition in a pair of mutants of Rd-apocyt b_{562}. These mutants were designed to fold in a two-state manner by significantly decreasing the stabilities of folded and intermediate states on the folding reaction coordinate, Figure 1. The observation of two-state folding provides, therefore, support of the proposed model for folding in this system.[24] The results of the present study allow placement of F61A/A90G and F61A/I72A on the folding energy diagram and the complete determination of the kinetics and thermodynamics of folding for these two mutants. The methodology can be applied to a large number of systems under nativelike conditions, providing dispersions in relaxation rates can be observed, and will therefore serve as a useful compliment to more traditional spectroscopic approaches for studying protein folding that often involve the use of denaturants.

Acknowledgment. We thank Dr. D. Korzhnev (University of Toronto) for many helpful discussions. W.-Y.C. was a recipient of a Senior Research Fellowship from the Canadian Institutes of Health Research (CIHR). This work was supported by a grant from the CIHR. L.E.K. holds a Canada Research Chair in Biochemistry.

JA042560U